Chapter 8

Reconstruction of neutral strange particles with ALICE

Hadrons K^0_S and Λ ($\overline{\Lambda}$) are unstable neutral primary particles that usually decay within the volume of the detector through the weak interaction. Their mean lifetimes are $\sim 2.7\,\mathrm{cm}/c$ and $\sim 7.9\,\mathrm{cm}/c$, respectively.[2] Their dominant decay channels, which are also used for their measurement, are:

$$\mathrm{K}^0_\mathrm{S} \to \pi^+ \pi^- \tag{8.1}$$

$$\Lambda \to p\,\pi^- \tag{8.2}$$

$$\overline{\Lambda} \to \bar{p}\,\pi^+ \ . \tag{8.3}$$

Because of how these hadrons' decay topologies appear in the detector (an undetectable neutral particle decaying into a V-shaped pair of detectable tracks), they are commonly nicknamed V0s[1].

8.1 Analysed datasets

TBA Description of data, collection years, some QA Monte Carlo The Monte Carlo data are simulated using a physics event generator (in this measurement, Pythia 8) and a model describing the propagation of particles through the detector environment (GEANT).

[1] Not to be confused with V0A and V0C—the forward calorimeters in ALICE, or V0M—the related multiplicity estimator using the calorimeters' signal.

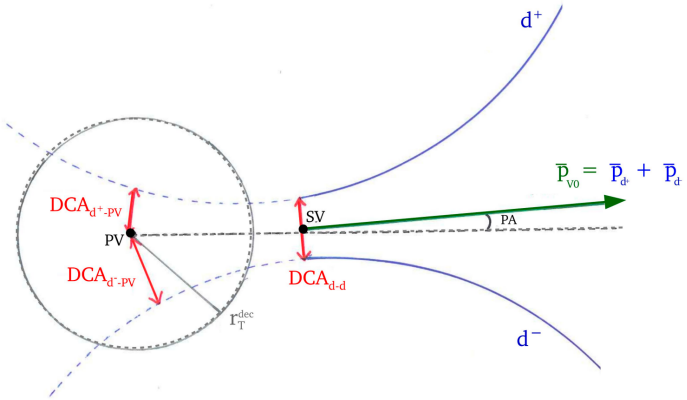

Figure 8.1: Typical topology of V0 decay. PV stands for primary vertex, SV for secondary vertex.? p. 102

8.2 Identification of V0s using ALICE

A centrally developed ALICE algorithm, the ALICE V0 finder, is used to collect suitable V0 candidates from pairs of oppositely charged tracks with the relevant topology. This typical topology is illustrated in Fig. ?? Additional selection criteria ("cuts") are further applied to suppress the background among those candidates. These include:

- cuts on kinematics of the mother and the daughters,
- constraints on the topology of the decay,
- constraints on the reconstruction quality of the daughter tracks,
- cuts on the specific ionisation energy loss of the daughters,
- rejection of contributions from pile-up using "fast detector" information,
- rejection of other competing V0 candidates based on their invariant mass.

The full list of used cuts is listed in Tab. ??.

8.3 Signal extraction

The V0 signal is separated from the background in distributions of M_{inv} in several p_{T} intervals using the so-called sideband method. Assuming the signal peaks around $\Delta m_{\text{V0}} = M_{\text{inv}} - M_{\text{V0}} = 0$ and approximating the background in this region as linear, the subsequent procedure is followed:

Table 8.1: Cuts used in the identification of the K^0_S, Λ, and $\overline{\Lambda}$ particles.

Cut Variable	Cut Value for K^0_S (Λ, $\overline{\Lambda}$)
Topology	
V^0 pseudorapidity	$-0.8 < \eta < 0.8$
Transverse momentum	$1.0 < p_\mathrm{T} < 25.0\ \mathrm{GeV}/c$
V^0 DCA	$\mathrm{DCA}^{\mathrm{d-d}} < 1.0$
Pointing angle	$\cos \mathrm{PA} > 0.97(0.995)$
Decay radius	$0.5\ \mathrm{cm} < R_{xy}$
Daughter Tracks Selection	
DCA of daughters to PV	$\mathrm{DCA}_{xy}^{\mathrm{d-PV}} > 0.06$ cm
TPC PID of daughters	$< 5\,\sigma$
Track pseudorapidity	$-0.8 < \eta < 0.8$
TPC crossed rows	$N_\mathrm{cr} > 70$
TPC crossed rows to findable ratio	$N_\mathrm{cr}/N_\mathrm{f} > 0.8$
Candidate Selection	
Proper lifetime (transverse)	$(R_{xy} \times m_{(\Lambda,\overline{\Lambda})}/p_\mathrm{T} < 30$ cm $)$
Competing mass	$> 4\,\sigma$

1. the sideband regions are defined. The M_inv spectra are fitted in the $-0.03 < M_\mathrm{inv} < -0.03\,\mathrm{GeV}/c^2$ interval using a χ^2-fit with the distribution

$$f = [0] + [1] \cdot M_\mathrm{inv} + [2] \cdot \mathcal{N}(\mu, \sigma_1^2) + [3] \cdot \mathcal{N}(\mu, \sigma_2^2)\ , \tag{8.4}$$

   where $\mathcal{N}$ is a Gaussian distribution. This is done in all p_T bins and illustrated in Fig. ??.

2. In each p_T bin, parameter σ is obtained as the RMS of $[2] \cdot \mathcal{N}(\mu, \sigma_1^2) + [3] \cdot \mathcal{N}(\mu, \sigma_2^2)$. To calculate the RMS, the distribution is sampled 10^5 times.

3. Variables μ_V0 and σ_V0 as functions of p_T are interpolated using χ^2 fit and the parametrisations:

$$\mu_{\mathrm{K}^0_\mathrm{S}}(p_\mathrm{T}) = \begin{cases} [0] + [1] \cdot p_\mathrm{T} + [2] \cdot p_\mathrm{T}^2 & \text{if } p_\mathrm{T} < 1.6\,\mathrm{GeV}/c, \\ [3] & \text{if } p_\mathrm{T} \geq 1.6\,\mathrm{GeV}/c, \end{cases} \tag{8.5}$$

$$\mu_{\Lambda,\overline{\Lambda}}(p_\mathrm{T}) = \begin{cases} [0] + [1] \cdot p_\mathrm{T} + [2] \cdot p_\mathrm{T}^2 & \text{if } p_\mathrm{T} < 1.9\,\mathrm{GeV}/c, \\ [3] + [4] \cdot p_\mathrm{T} & \text{if } p_\mathrm{T} \geq 1.9\,\mathrm{GeV}/c, \end{cases} \tag{8.6}$$

$$\sigma_\mathrm{V0}(p_\mathrm{T}) = [0] + [1] \cdot p_\mathrm{T} + \frac{[2]}{p_\mathrm{T}}\ . \tag{8.7}$$

   The fitted parametrisations can be seen in Fig. ??.

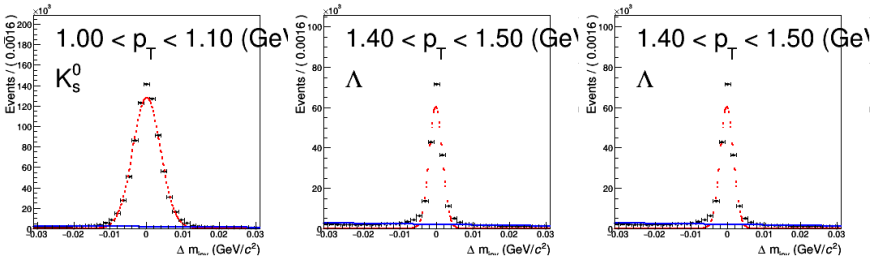

Figure 8.2: Determination of the signal peak mean and width using a fit of the Gaussian distribution for K^0_S, Λ, and $\overline{\Lambda}$ particles.

4. In each p_T bin, we define the signal region **N** as $(\mu_{\mathrm{V0}} - 6\sigma_{\mathrm{V0}}; \mu_{\mathrm{V0}} + 6\sigma_{\mathrm{V0}})$ and the sidebands **A** and **B** as $(\mu_{\mathrm{V0}} - 12\sigma_{\mathrm{V0}}; \mu_{\mathrm{V0}} - 6\sigma_{\mathrm{V0}})$ and $(\mu_{\mathrm{V0}} + 6\sigma_{\mathrm{V0}}; \mu_{\mathrm{V0}} + 12\sigma_{\mathrm{V0}})$. In these regions, we sum together the entries and acquire N, A, B. The choice of $6\sigma_{\mathrm{V0}}$ is rather liberal to avoid biases from incorrect determination of the μ_{V0} or the imperfect description of the signal peak width σ_{V0}

5. Since the background is assumed to be linear, the sum of the two sideband integrals is an accurate estimation of the background in the signal region. Particle yields Y and the corresponding statistical uncertainties σ_Y are calculated as

$$Y = N - A - B \tag{8.8}$$

$$\sigma_Y = \sqrt{N + A + B}\ , \tag{8.9}$$

due to the fact that the statistical uncertainties in the signal and sideband regions are fully uncorrelated. Illustrations of this step can be seen in Fig. **??**.

8.3.1 Validation using simulations

The accuracy of the sideband method is tested with "MC closure"—in MC simulated data, the p_T-spectra acquired blindly from the V0 candidates are compared with p_T-spectra of identified V0. The ratios can be seen in Fig. **??** and show a $\sim 5\%$ effect at high-p_T. This is caused by the fact that in ALICE MC simulations, the V0 mass peaks have somewhat longer tails than in data and thus the signal can enter the background regions. This has to be taken into account when defining reconstruction efficiency using MC data.

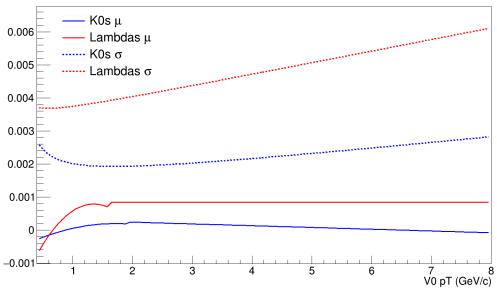

Figure 8.3: Parametrisation of the signal peak mean and width as a function of p_{T}.

Alternative approach

Originally, methods involving a likelihood fit and an unbinned likelihood fit of two Gaussian distributions as well as other background descriptions were tested. However, although more sophisticated, these methods proved considerably less precise. This is due to the fact that the signal peaks cannot be accurately described by the two Gaussian distributions, particularly in highly populated p_{T} bins. That said, they are sufficient to determine the σ_{V0} for above-stated purposes.

Mass resolution of secondary Λ and $\overline{\Lambda}$ particles

Approximately 20% of the Λ yields measured are produced as secondary particles coming from decays of the Ξ baryon in most cases – also called feeddown. Investigations of the simulated data revealed that the invariant mass of these secondaries suffers from a worse resolution (ca. 3 times higher σ). Subsequently, this gives our signal extraction a ca. 75% efficiency for secondaries, and ca. 95% efficiency for inclusive Λ yields at intermediate p_{T}. This has to be taken into consideration when calculating corrections for the feeddown yields. This effect can be seen in Fig. ??.

8.4 Normalisation

The reconstructed $\mathrm{K}^0_{\mathrm{S}}$, Λ, and $\overline{\Lambda}$ yields $Y(\eta, p_{\mathrm{T}})$ are normalised according to

$$\frac{\mathrm{d}^2 N^{\mathrm{raw}}}{\mathrm{d}y \mathrm{d}p_{\mathrm{T}}} = \frac{1}{N_{\mathrm{ev}}} \frac{1}{J} \frac{1}{\Delta\eta} \frac{1}{\Delta p_{\mathrm{T}}} Y(\eta, p_{\mathrm{T}}) \quad , \tag{8.10}$$

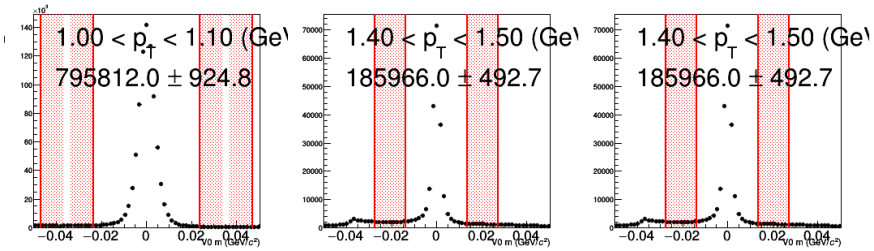

Figure 8.4: Visualisation of the sideband regions, from which the background is estimated, for K^0_S, Λ, and $\overline{\Lambda}$ particles.

where N_ev is the number of selected events, J the Jacobian of the $\eta \to y$ transformation, and $\Delta\eta$ and Δp_T the widths of the pseudorapidity and transverse momentum intervals, respectively.

TBA Jacobian

TBA Event loss correction

8.5 Corrections to the reconstructed production

To acquire results with scientific relevance, the raw yields of V0s observed with ALICE need to be corrected for geometrical acceptance, detector effects, and, in the case of Λ ($\overline{\Lambda}$), also for secondary contribution.

8.5.1 Secondary contribution correction

Only ca. 80% of the measured inclusive Λ and $\overline{\Lambda}$ yields are produced directly in the pp collision or near-instantanously in non-weak decays of resonances, as primary particles. The remainder is produced secondarily, as products of weak decays of heavier baryons. The dominant, and the only relevant, reactions are:

$$\Xi^- \to \Lambda\,\pi^- \ , \tag{8.11}$$

$$\Xi^0 \to \Lambda\,\pi^0 \ , \tag{8.12}$$

$$\Xi^+ \to \overline{\Lambda}\,\pi^+ \ , \tag{8.13}$$

$$\overline{\Xi}^0 \to \overline{\Lambda}\,\pi^0 \ . \tag{8.14}$$

For the K^0_S, the secondary production (such as from ϕ mesons) is negligible.

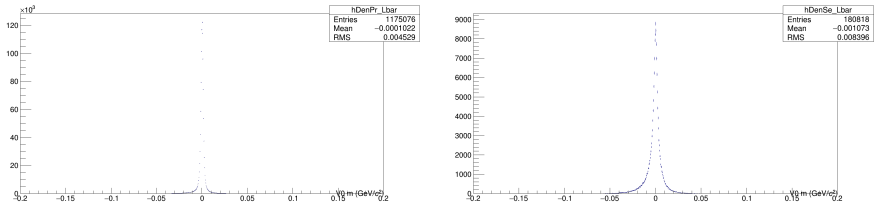

(a) (b)

Figure 8.5: TBA.

The primary Λ yields can be estimated using the following equation,

$$\Lambda^{\mathrm{raw}}_{\mathrm{primary}}(p^i_{\mathrm{T}}) = \Lambda^{\mathrm{raw}}_{\mathrm{measured}} - \Lambda^{\mathrm{raw}}_{\mathrm{secondary}} \tag{8.15}$$

$$= \Lambda^{\mathrm{raw}}_{\mathrm{measured}} - \sum_j F^{\Lambda}_{ij} \int_{p^j_{\mathrm{T}}} \frac{dN}{dp_{\mathrm{T}}}(\Xi^-) \quad , \tag{8.16}$$

where F_{ij} is the so-called feeddown matrix giving the probabilities of a produced Ξ^- or Ξ^0 particle in a p_{T} interval j decaying into reconstructed Λ in a p_{T} interval i, and $\frac{dN}{dp_{\mathrm{T}}}(\Xi^-)$ the measured Ξ^- spectra. This approach assumes that the Ξ^0 decay contribution is identical to Ξ^- and is used because Ξ^0 baryons are challenging to measure. For the $\overline{\Lambda}$, the equation is analogous but uses Ξ^+ .

The feeddown matrix is calculated in ALICE MC simulations of MB events,

$$F^{\Lambda}_{ij} = 2 \cdot \frac{N_{\mathrm{rec.}}(\Lambda)|^{p^{\Xi}_{\mathrm{T}}=j}_{p^{\Lambda}_{\mathrm{T}}=i}}{N_{\mathrm{gen.}}(\Xi)|_{p^{\Xi}_{\mathrm{T}}=j}} \quad , \tag{8.17}$$

where Ξ represent both Ξ^- and Ξ^0. There is an assumption that the probabilities, and thus, the matrix, do not depend on multiplicity of the event. It is taken into account in systematic uncertainties.

An alternative approach is constructing F^{Λ}_{ij} from charged Ξ solely, and then multiplying $\Lambda^{\mathrm{raw}}_{\mathrm{secondary}}$ by two and was used to determine the systematic uncertainty.

As discussed previously, due to the worse mass resolution of secondary Λ, a M_{inv} cut of $5\sigma_{\mathrm{V0}}$ (determined in the sideband definition procedure). Since a large amount of the secondaries enter the background regions, a negative weight -1 has to be applied to achieve the best MC closure validation. Other configurations ($6\sigma_{\mathrm{V0}}$ and -1 weight, $4\sigma_{\mathrm{V0}}$ and 0 weight) were also tested.

The feeddown matrices F^{Λ}_{ij}, $F^{\overline{\Lambda}}_{ij}$ are displayed in Fig. ??.

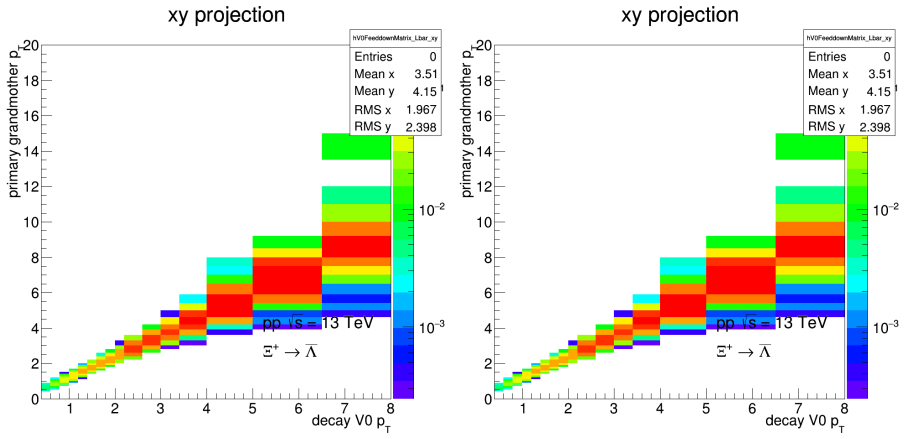

(a) (b)

Figure 8.6: Feeddown matrices **(a)** F_{ij}^{Λ} and **(b)** $F_{ij}^{\overline{\Lambda}}$ from Ξ baryons.

Ξ spectra

Fitting. TBA

8.5.2 Reconstruction efficiency

The total reconstruction efficiency, including the acceptance, for V0s in our events with ALICE can be determined using the Monte Carlo simulated data. It is calculated as

$$\epsilon(p_{\mathrm{T}}) = \text{acceptance} \times \epsilon_{\text{rec}} \tag{8.18}$$

$$= \frac{\#\,\text{associated reconstructed V0s}}{\#\,\text{generated V0s within}\,|\eta| < 0.8}\,, \tag{8.19}$$

in events that passed the selection criteria. The association is done by comparing the mother's and daughters' PDG ID as well as the MC generator label. Particles in the numerator have to satisfy all selection cuts. The reconstruction efficiency for $\mathrm{K}^0_{\mathrm{S}}$, Λ, and $\overline{\Lambda}$ is plotted in Fig. ??.

As mentioned before, in ALICE simulations, the M_{inv} resolution worsens with increasing p_{T}; in high-p_{T} bins, the simulated V0s are sometimes reconstructed with higher M_{inv} than what is considered realistic. This would lead to a lower efficiency as those V0s can fall out of the signal region, and an overestimation of the total measured spectra. For this reason, a $4\sigma_{\mathrm{V0}}$ cut is required for the V0s M_{inv} in the numerator.

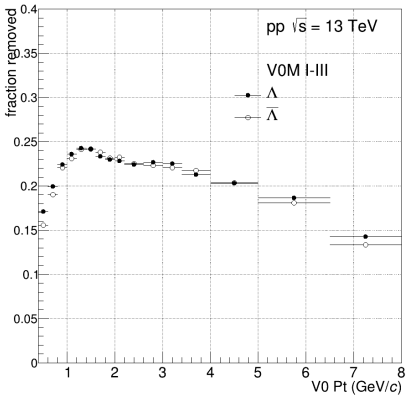

Figure 8.7: TBA.

Alternatively, one could use a cut of $6\sigma_{\mathrm{V0}}$ and applying a negative weight -1 in cases where it is not satisfied.

The reconstruction efficiency is defined in MB events, assuming the reconstruction in pp collisions does not largely depend on multiplicity, geometrical event classification, or event sub-structure. This assumption is taken into account in systematic uncertainties.

8.6 Transverse momentum spectra

Using the corrections on the normalised yields, one acquires the measured transverse momentum spectra, which are comparable with production cross sections and thus theoretical predictions.

$$\frac{\mathrm{d}^2N}{\mathrm{d}y\mathrm{d}p_{\mathrm{T}}} = \epsilon(p_{\mathrm{T}}) \times \frac{\mathrm{d}^2N^{\mathrm{raw}}_{\mathrm{primary}}}{\mathrm{d}y\mathrm{d}p_{\mathrm{T}}} \tag{8.20}$$

8.6.1 Comparisons with previously published results

The acquired results were tested against previously published measurements of $\mathrm{K}^0_{\mathrm{S}}$, Λ, and $\overline{\Lambda}$ transverse momentum spectra at the ALICE experiment in MB as well as high-multiplicity (V0M I and V0M III) events in pp collisions at $\sqrt{s} = 13$ TeV.

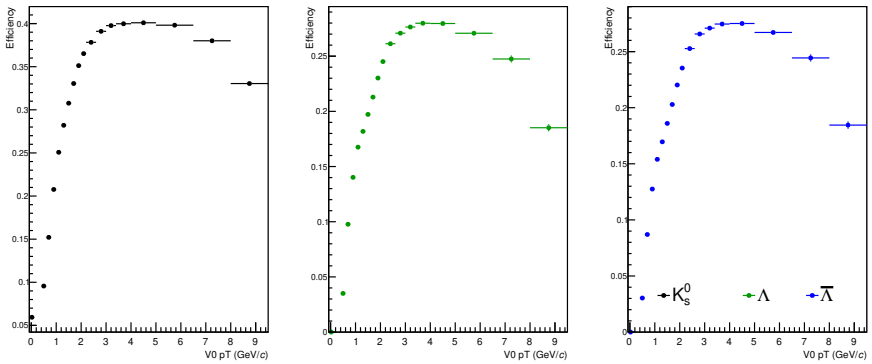

Figure 8.8: TBA.

K^0_S

The published K^0_S results were measured in `kINT7` events. Thus, in order to compare on an equal footing, a trigger efficiency scaling factor $\epsilon_{\text{trig}} = 0.7448$, taken over from, was applied to this analysis.

The comparison of this analysis to the published results can be seen in Fig. ??a. In high-multiplicity events, the spectra are in a good agreement across the entire p_{T} range (most points lie within $\sim 5\%$ difference). In MB events, there is a difference ($\sim 10\%$) at the lowest p_{T} values. This is understood as a loss of signal in events with no reconstructed charged tracks and is usually corrected for. Since the correction plays a role only in MB – events which are of little interest to this thesis' work – it is not taken into account.

Λ + $\overline{\Lambda}$

The published Λ + $\overline{\Lambda}$ results were measured in same events as this analysis, (`INEL>0`), therefore, ϵ_{trig} was not applied. They are compared to this analysis in Fig. ??b and show a satisfactory agreement (most points lie within $\sim 5\%$ difference).

8.7 Systematic uncertainties

Experimentally measured values always come with uncertainties – statistical and systematic. Whereas statistical uncertainties are caused by the limited number of measurements and can be decreased by increasing the statistical sample analyzed, system-

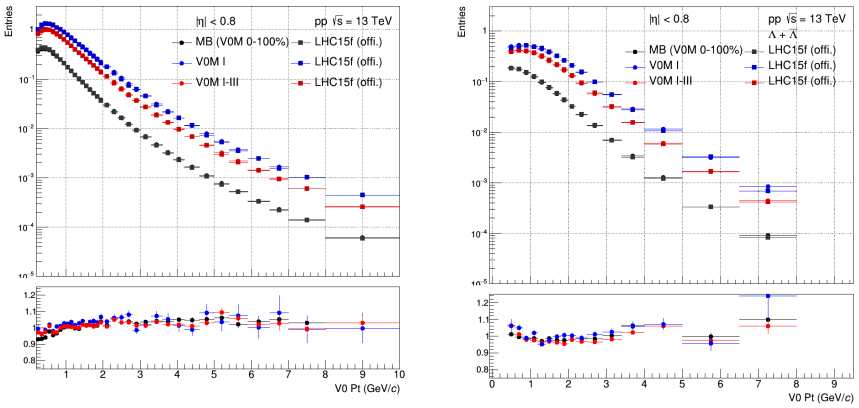

(a) (b)

Figure 8.9: Cross-checks of this analysis' p_{T} spectra of **(a)** $\mathrm{K}^0_{\mathrm{S}}$ and **(b)** $\Lambda + \overline{\Lambda}$ in MB, $\mathrm{V0M}$ I, and $\mathrm{V0M}$ I-III events in pp collisions at against $\sqrt{s} = 13$ TeV results previously published by ALICE.

atic uncertainties represent the imprecision or the bias of the experimental methodology itself. Calculation of statistical uncertainties is given directly from frequentist statistics. Definition of systematic uncertanties, however, is not always straightforward – one cannot simply re-do the measurement with several completely different experimental setups and data analysis techniques. Therefore, a lot of effort needs to go into identifying all possible sources of systematic uncertainties.

In this measurement, the following sources of systematic uncertainty were identified as relevant:

- **Variation of selection criteria**
  In determining the reconstruction efficiency, it is assumed that in ALICE MC simulations, all observables used for the identification of V0s and for assuring the quality of daughter tracks represent reality. Their inaccurate description, however, results in a bias. This bias is estimated by testing the sensitivity of the final results to varying the selection criteria on these observables.

- **Signal extraction method**
  The biases of the sideband background estimation procedure are tested against increasing and reducing the signal and background regions, by varying the number of σ_{V0}. Variations of 5 and 7 σ_{V0} were used.

- **Multiplicity dependence of $\epsilon(p_{\mathrm{T}})$**
  Studies of the reconstruction efficiency in pp collisions reveal a small, albeit

significant dependence on the collision final state. A constant uncertainty of $\sim 2\%$ is applied on the spectra to account for this.

- **Feeddown correction**
  Three sources of uncertainty on the contribution of secondary particles were identified – variation of the Ξ yields, multiplicity dependence of the feeddown matrix, and an alternative method.

- **Material budget**
  This uncertainty reflects that implementing ALICE's material composition in simulations comes with limitations. Previous studies in ALICE which varied parameters of the description of the apparatus showed that this effect corresponds to a constant 4% uncertainty on the measured spectra.

When testing the default method A against an alternative method B, one can implement the deviation of the ratio of their measured values $\Delta = B/A$ from unity as an uncertainty. To ensure that this difference is statistically significant and not just an effect of a limited data sample, the deviation is considered only if it exceeds its own uncertainty, defined as

$$\sigma_\Delta = \frac{\sqrt{|\sigma_B^2 - \sigma_A^2|}}{A} \quad , \tag{8.21}$$

where σ_A and σ_B are the uncertainties of the results from methods A and B, respectively.

8.7.1 Variation of selection criteria

To investigate the differences between description of variables in measured data and ALICE simulations, and determine sensible cut variations λ_i, raw yield loss F was studied. It was measured in MB events and defined as

$$F(\lambda) = 1 - \frac{Y(\lambda)}{Y(\lambda_0)} \quad , \tag{8.22}$$

where $Y(\lambda)$ is the raw yield as a function of the cut value λ and $\lambda_{\mathrm{LOOSEST}}$ the loosest variation (corresponding to the highest yield).

For most observables, the systematic effect can be estimated from alternative methods using $\lambda_{\mathrm{LOOSEST}}$ and $\lambda_{\mathrm{TIGHTEST}}$. To ensure the stability and possible non-linearity, less strict λ_{LOOSE} and λ_{TIGHT} are also tested. If applicable t is reasonable to choose λ_i such that $F(\lambda_i)$ does not exceed approximately 10%.

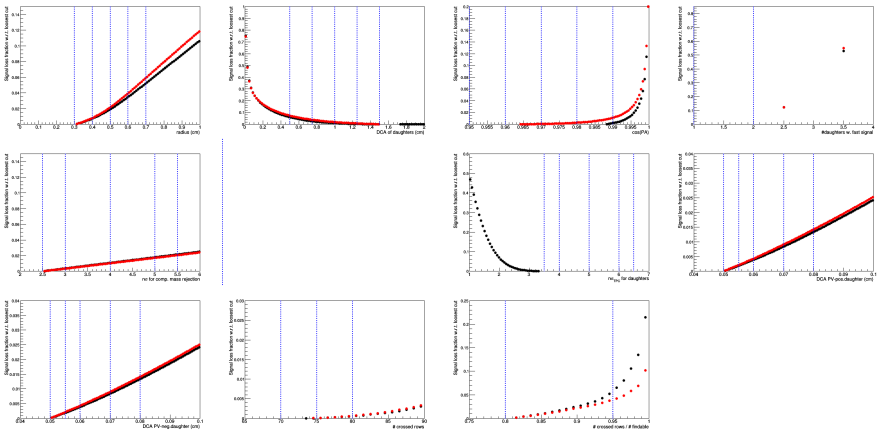

Figure 8.10: TBA

The $F(\lambda)$ for the different selection critera, and with the chosen λ_i are shown in Fig. **??**, Fig. **??**, and Fig. **??** for K^0_S, Λ, and $\overline{\Lambda}$, respectively. The pile-up rejection cut, which requires "fast detector" information for at least one daughter is of a binary nature. So, its variation was tested by requiring a different amount of "fast detector" hits between the two daughters. The selected values of λ_i are summarised in Tab. **??**.

Table 8.2: Cut variation parameters for the K^0_S (Λ and $\overline{\Lambda}$).

Quality	loosest	loose	default	tight	tightest
radius	0.3	0.4	0.5	0.6	0.7
DCA between daughters	1.5	1.25	1.0	0.75	0.5
cos PA	0.95 (0.993)	0.96 (0.994)	0.97 (0.995)	0.98 (0.996)	0.99 (0.997)
pile-up removal cut	-	-	1	2	-
comp. mass number of σ	2.5	3.0	4.0	5.0	5.5
lifetime	-	(35.0)	(30.0)	(25.0)	-
TPC PID number of σ	6.5	6.0	5.0	4.0	3.5
DCA to PV of pos. track	0.05	0.055	0.06	0.07	0.08
DCA to PV of neg. track	0.05	0.055	0.06	0.07	0.08
TPC crossed rows	-	-	70	75	80
TPC find. ratio	-	-	0.8	0.95	-

8.7.2 Feeddown correction

As mention before, first, the Ξ spectra, from which the feeddown is calculated, are varied within their reported uncertainties. In both variations, the yields are then extracted using a fit. Second, similarily to $\epsilon(p_T)$, the assumption of no multiplicity

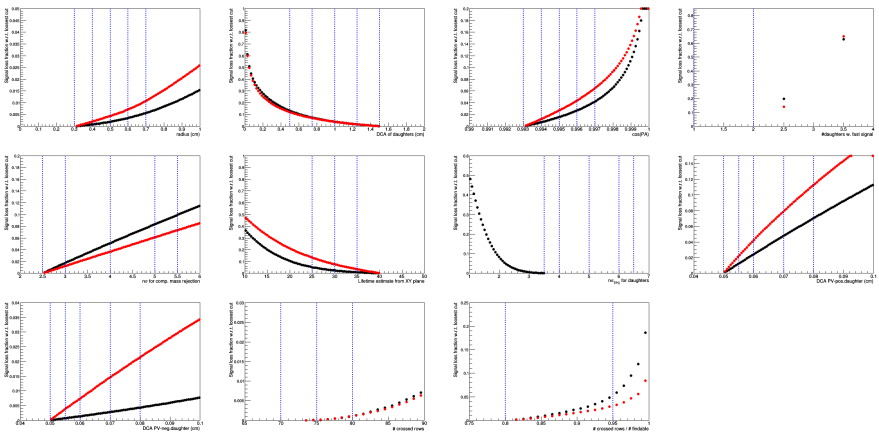

Figure 8.11: TBA

dependence of the feeddown matrix is accompanied by a constant uncertainty of 2% on the secondary yields (corresponding to ca. 0.6% uncertainty on the primary yields).

Lastly, an alternative method of estimating the feeddown just from charged Ξ baryons, and multiplying by a factor of two, was also tested and contributes a systematic uncertainty. It is considered significant and applied when $|\Delta - 1| > \sigma_{\Delta}$. The difference between the two methods can be seen in Fig. **??**. It should be noted that whilst the secondary yields suffer from a rather large systematic uncertainty, the effect on the primary spectra is significantly smaller, as the uncertainties enter as $\frac{1-B}{1-A}$ and the secondary yields do not exceed $\sim 30\%$.

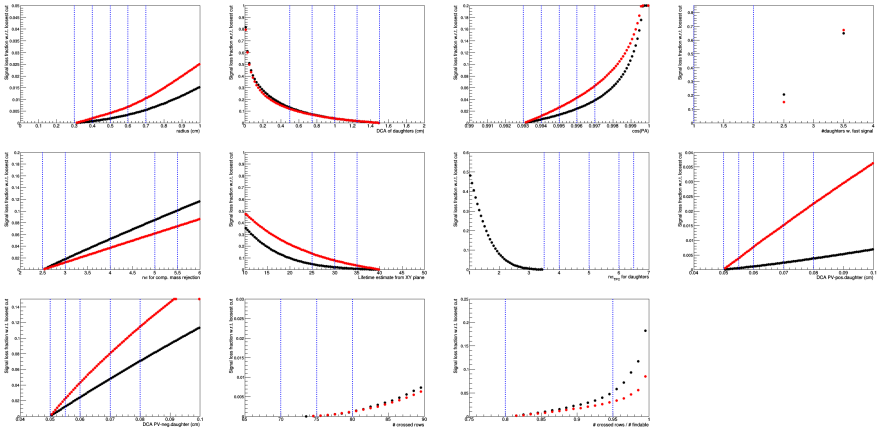

Figure 8.12: TBA

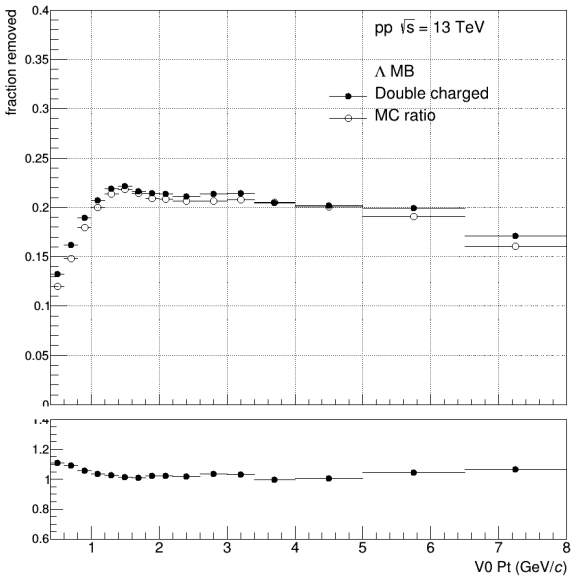

Figure 8.13: TBA